Role of Nucleus Accumbens in Neuropathic Pain: Linked Multi-Scale Evidence in the Rat Transitioning to Neuropathic Pain

Pei-Ching Chang[1,†], **Sarah Lynn Pollema-Mays**[1,†], **Maria Virginia Centeno**[1], **Daniel Procissi**[2], **Massimos Contini**[3], **Alex Tomas Baria**[1], **Macro Martina**[1], and **Apkar Vania Apkarian**[1,*]

[1]Department of Physiology, Northwestern University Feinberg School of Medicine, Chicago, Illinois 60611, USA.

[2]Department of Radiology, Northwestern University Feinberg School of Medicine, Chicago, Illinois 60611, USA.

[3]Dipartimento di Scienze Fisiologiche, Universita` di Firenze, I-50134, Firenze, Italy.

Abstract

Despite recent evidence implicating the nucleus accumbens (NAc) as causally involved in the transition to chronic pain in humans, underlying mechanisms of this involvement remain entirely unknown. Here we elucidate mechanisms of NAc reorganizational properties (longitudinally and cross-sectionally), in an animal model of neuropathic pain (spared nerve injury, SNI). We observed inter-related changes: 1) In resting-state fMRI, functional connectivity of the NAc to dorsal striatum and cortex was reduced 28 days (but not 5 days) after SNI; 2) contralateral to SNI injury, gene expression of NAc dopamine 1A, 2, and κ-opioid receptors decreased 28 days after SNI; 3) In SNI (but not sham) covariance of gene expression was upregulated at 5 days and settled to a new state at 28 days; and 4) NAc functional connectivity correlated with dopamine receptor gene expression and with tactile allodynia. Moreover, interruption of NAc activity (via lidocaine infusion) reversibly alleviated neuropathic pain in SNI animals. Together, these results demonstrate macroscopic (fMRI) and molecular reorganization of NAc and indicate that NAc neuronal activity is necessary for full expression of neuropathic pain-like behavior.

Introduction

Concepts regarding the role of nucleus accumbens (NAc) in pain, and in chronification of pain, are undergoing rapid advances. Until recently this nucleus was thought to be primarily involved in evaluating reward signals, yet new evidence shows that it also encodes salience for pain, and value for pain relief and that NAc valuation of acute analgesia is distorted in chronic pain patients [9; 12; 13; 54; 64; 65]. Recent evidence indicates that increased

[*]To whom correspondence should be addressed to Dr. A. Vania Apkarian (a-apkarian@northwestern.edu). Address: Northwestern University, 303 East Chicago Avenue, Tarry Bldg. 7-705, Chicago, Illinois 60611, USA. Phone Office: (312) 503-0404. Fax: (312) 503-5101.
[†]These authors equally contributed to the study.

functional connectivity between NAc and the prefrontal cortex is predictive of the transition from acute to chronic pain one year prior to pain chronification [10]. Despite these advances, the mechanistic implications of the macroscopic human brain imaging-based findings remain unknown; even though they were predicated on the hypothesis that NAc dopaminergic learning mechanisms may play an essential role in pain chronification [7].

The NAc is a central component of the mesocorticolimbic system [5; 19; 31]; a brain network closely associated with emotional learning, motivated and addictive behavior, in which dopaminergic neurotransmission and modulation are thought to supply the critical learning signal. Knowledge of the role of the mesolimbic circuitry in pain is increasing. The association between mesolimbic circuitry and neural substrates of pain and analgesia has been considered in the past decades [29; 37; 53]; for noxious or aversive conditions both excitatory and inhibitory responses of dopaminergic neurons have been observed [16; 23; 43; 50; 62; 68], both increases and decreases in extracellular dopamine are reported [11; 51], and corresponding results are found in human studies [44; 46]. Moreover, in patients with central disorders such as schizophrenia, Parkinson's disease, substance abuse, and mood and anxiety disorders, pain sensitivity is altered, presumably as a consequence of changes in the dopaminergic system [1; 42; 71], and animal studies implicate dopamine in acute and neuropathic conditions [6; 26; 60]. Yet, the mechanistic role of NAc in pain chronification remains unknown.

The present study was designed to interrogate NAc properties in the spared nerve injury (SNI) model of neuropathic pain to evaluate cross-species correspondences, and to inform the relationship between fMRI macroscopic measures and related molecular mechanisms. The SNI model is a robust rodent model of neuropathic pain in which animals develop lifelong pain following nerve injury. It is used here as a tool for detecting how persistent neuropathic pain may affect the NAc. Given that the critical role of NAc in human pain chronification was identified in a combined longitudinal and cross-sectional study, we adopted a similar approach in the rat and tracked NAc functional connectivity and receptor properties, as animals transitioned from healthy to neuropathic pain behavior. Furthermore, we examined the effects of reversibly interrupting NAc activity on modulation of neuropathic behavior.

Methods

Animals

Adult male Sprague Dawley rats (Harlan, Indianapolis, IN; 200 – 250g) were used throughout the experiments. Animals were housed on soft bedding in groups of three per cage on a 12-h light/dark cycle in a temperature-controlled environment ($21 \pm 2°C$) with food and water available *ad libitum*. For all animals, handling and testing were performed during the light period. To minimize stress, they were handled regularly before injury and before behavioral testing. All experimental procedures were approved by the Northwestern University Institutional Animal Care and Use Committee. Behavioral measures and initial fMRI data analyses were performed in a blinded fashion.

Experimental Design

Experiment A—In this experiment, we tested how peripheral nerve injury induces changes in NAc due to persistent neuropathic pain. We tracked NAc properties cross-sectionally (in comparison to sham animals) from pre-injury (Day-2) to persistent pain (Day5 and Day28), using mRNA receptor expression, fMRI functional connectivity, and behavior. The experimental paradigm is summarized in Fig. 1A. Animals were divided into two groups: the Short Term group sacrificed at Day5, and the Long Term group sacrificed at Day28 (MRI: Day5: SNI = 10, sham = 12 animals; Day28: SNI = 13, sham = 11 animals. RT-qPCR: Day5: SNI = 14, sham = 13 animals; Day28: SNI = 14, sham = 12 animals). Because physiological recording was used for fMRI data pre-processing, rats with incomplete physiological recordings during the scans were excluded from the fMRI study; however these rats were still included in the receptor gene expression analysis. fMRI data was obtained before injury, as well as on the day before they were sacrificed to extract NAc tissue for mRNA receptor expression. Mechanical allodynia was assessed the day before each fMRI scan.

Experiment B—Modulation of neuropathic behavior was investigated by blocking NAc activity using a brain microinjection technique. A different set of SNI animals received chronic infusion of lidocaine 2% (n = 8) or saline as vehicle control (n = 7) in the NAc for 14 days. The experimental paradigm is summarized in Fig. 2. An Alzet mini pump was implanted on the side (right) contralateral to the paw (left) that received SNI injury, with both procedures performed on the same day. Behavioral tests for mechanical and cold allodynia were assessed twice before injury (around Day-2 for implanting the pump and injuring the peripheral nerve) as well as on Day4, Day7, Day10, Day14, Day17 and Day20.

Spared Nerve Injury (SNI)

SNI was used as an animal model of persistent peripheral neuropathic pain. The SNI model has been described previously [24]. Animals were anesthetized with isoflurane (1.5 –2%) and a mixture of 30% N_2O and 70% O_2. The sciatic nerve of the left hind leg was exposed at the level of trifurcation into the sural, tibial, and common peroneal nerves. The tibial and common peroneal nerves were tightly ligated and severed, leaving the sural nerve intact. Animals in the sham injury group served as the control as their sciatic nerves were exposed, as in the SNI procedure, but they received no further manipulations.

Test for Mechanical Allodynia

Tactile sensitivity of the hind paw was measured using withdrawal responses to a series of von Frey filaments as previously described [20]. Animals were placed in a Plexiglass box with a wire grid floor and allowed to habituate to the environment for 10 – 15 minutes. Filaments of varying forces (Stoelting Co, USA) were applied to the lateral part of the plantar surface of the hind paw. Filaments were applied in either ascending or descending strengths to determine the filament strength closest to the hind paw withdrawal threshold. Each filament was applied for a maximum of 2 seconds at each trial; paw withdrawal during the stimulation was considered a positive response. Given the response pattern and the force of the final filament, 50% response threshold (in grams) was calculated [20].

Test of Cold Allodynia

The measurement of sensitivity to cold consisted of applying 1 drop (about 50μl/site) of acetone solution on the lateral hind paw of the animal as previously described [22]. The withdrawal reaction of the animals was observed. Half a second and 20 seconds were assigned as minimal and maximal cut-off points, respectively. This test was repeated three times per paw, at 10-minute intervals. A score ranging from 0 to 4 was used to quantify the type of reactions (withdrawal, vocalization, flinching and licking) the animals exhibited to the acetone drop. The scores of an animal's reactions during three times of the test were averaged for per paw, and used as the score of the animal.

MRI Acquisition

All MR experiments were carried out on a Bruker 7 T/40 cm horizontal magnet (Clinscan, Bruker Biospin, Ettlingen, Germany) with a surface coil. Blood oxygen level-dependent (BOLD) contrast-sensitive T2*-weighted gradient-echo echo-planar images were acquired for resting state fMRI (rs-fMRI) scans. Each scan consisted of 300 volumes of 14 slices acquisition (repetition time (TR) of 1.3 seconds, echo time (TE) of 25 milliseconds, flip angle $= 60°$, 1.0 mm slice thickness, and 0.5×0.5 mm^2 in-plane resolution). A high-resolution T2-weighted RARE anatomical reference was acquired for each animal (1.0 mm slice thickness and 0.273×0.273 mm^2 in-plane resolution). An additional T2-weighted RARE anatomical scan with the same geometry as the functional image (1 mm slice thickness and 0.5×0.5 mm^2 in-plane resolution) was also acquired and used as a low-resolution anatomical reference.

Anesthesia was induced and maintained during the experiments with isoflurane (1.75 – 2.5%) mixed with air. Body temperature, respiratory rate, and heart rate were monitored and recorded during scans (Model 1025; SA Instruments, Stony Brook, NY, USA). The monitoring system was operated using a fiber optic temperature probe, respiration pad and fiber optic pulse oxymeter. Respiratory and cardiac waves were recorded during image acquisition with a temporal resolution of 0.001 kHz. To maintain body temperature around 37°C during the imaging session, a feedback-controlled water circulation system (medres, Cologne, Germany) was used to supply the base of the cradle. rs-fMRI scans were collected only when physiological parameters remained stable for about 10 minutes.

Image Preprocessing

The rs-fMRI data was preprocessed with AFNI (http://afni.nimh.nih.gov) and FSL 5.1 (FMRIB's Software Library, http://www.fmrib.ox.ac.uk/fsl). The fMRI were first skull stripped and preprocessed using AFNI by applying de-spiking, removal of physiological artifacts from respiration and heartbeat, and correction for slice timing. Rats that had incomplete respiratory and cardiac recordings were discard from MRI data analysis. The images were then processed using FSL for correction for motion, spatially smoothed with a Gaussian kernel of 0.8 mm FWHM and high pass filtered with a cutoff of 100 seconds.

Volumes from functional images were registered to a standard space with a three-step process. Images were first aligned with the individual's low-resolution anatomical image followed by alignment with the individual's high-resolution anatomical image, and then co-

registered to a standard space. Average time courses from all of the voxels inside whole brain, white matter (WM) and cerebrospinal fluid (CSF) were extracted. Confounding regressors that modeled global whole brain, WM and CSF signals and six motion parameters, including translations and rotations, were removed from images through linear regression.

Functional Connectivity Analysis

rs-fMRI connectivity was evaluated using a seed-based correlational approach. Based on histological characteristics in animals, the NAc is divided into two major sub-territories, the core and the shell [27; 41; 48]. Fig. 3A displays the coordinates of seeds for the NAc core and shell, which were selected based on the rat MRI atlas [63] and were used for functional connectivity analysis. Averaged time course from all of the voxels inside the seed region was correlated with every other voxel time course of the brain. Correlation coefficients (r) were converted to a normal distribution using Fisher's z transform (z(r)). In order to evaluate anesthesia-related global functional connectivity [47], 1000 randomly selected voxels were correlated with every other voxel time course of the brain, Fisher's z transformed, and averaged to yield a single index per animal, which represented the anesthesia-related global functional connectivity of the animal. No significant difference was found between the indices of SNI and sham animals for all experimental conditions (Day-2, Day5 and Day28). To diminish anesthesia-related across animal variability, global functional was used as confounding regressor in the group-level statistical analysis.

Voxel-wise group-level statistical analysis of functional connectivity were assessed non-parametrically using the FSL Randomize tool [55]. For each analysis, 5000 random permutations were carried out. The analyses were performed only within the gray matter mask. All statistical maps were family-wise error (FWE) corrected using $P < 0.05$, based on the threshold-free cluster enhancement (TFCE) statistic image [66].

Gene Expression Analysis

Gene expression was performed on NAc from SNI and sham operated rats at Day5 and Day28. Rats were deeply anesthetized with Isoflurane and rapidly decapitated; brains were removed while immersed in TBS frozen buffer. Brains were sliced coronally from Bregma 2.20 to 1.00, allowing easy visualization of the NAc, and contralateral and ipsilateral NAc were removed separately and frozen in liquid nitrogen, and stored at − 80°C. RNA was extracted using a Qiagen RNeasy RNA extraction kit; DNA contamination was prevented by first using a column that binds DNA while allowing RNA to flow through. RNA was reverse transcribed into cDNA using Roche's First Strand cDNA Synthesis kit and oligo dT primers. RNA yield and quality was confirmed with Nanodrop analysis.

RT-qPCR was done using a Roche Lightcycler 480 (LC480) with either Roche probes master mix or SYBR green master mix, primers (0.4 μM), hydrolysis probes and NAc cDNA (primers listed in Table S7). All genes of interest were normalized to the GAPDH reference gene. For hydrolysis probe reactions, a single gene of interest was multiplexed with the reference gene GAPDH in the same well. Reactions consisted of a 5-minute hot start incubation at 95°C, followed by 45 cycles of 10-second at 95°C, 10-second at 60°C,

and 1-second at 72°C. Primers were initially validated using a SYBR green RT-qPCR assay, which allowed for melting temperature analysis, demonstrating a single peak for each gene product. RT-qPCR samples were also run on 1.8% agarose gels to verify single gene products. Although primers were intron spanning, cDNA negative and reverse transcriptase negative controls were done for genes of interest and did not give a signal. As recommended in published guidelines for RT-qPCR methods, all data were efficiency corrected [18]. Standard curves were done to calculate reaction efficiency for each gene product using dilutions of NAc cDNA. All data were efficiency corrected using Roche LC480 software and the delta delta Ct method [61]. For multiplex reactions, efficiency curves were run using multiplex parameters, while for SYBR green reactions efficiency curves were done with SYBR green reaction mixes. Within the recommendations of the MIQE RT-qPCR guidelines, a reference gene can be validated by running another reference gene against it. Thus to validate GADPH as a stable reference gene, tubulin was run relative to GAPDH for all samples and no differences in tubulin were detected when run against GAPDH. According to MIQE guidelines this provides sufficient confidence in GAPDH that it can be used as a reference gene on its own [18]. Statistical analyses were done using a two-way ANOVA test, with Fisher LSD for post-hoc analysis.

Correlation Analysis

Relationships between NAc functional connectivity, receptor expression, and pain behavior were investigated using correlation analysis. Data for correlation analysis were pooled from Day5 and Day28, separately for SNI and sham animals. For inter-run calibration for RT-qPCR, a normalized receptor gene expression was used in the correlation analysis. The samples of brain tissue were tested for RT-qPCR in two runs, with each run consisting of SNI and sham animals at Day5 and Day28. Thus, a z-score of receptor gene expression was calculated with each run in order to calibrate the two runs.

Mini-Pump Insertion

Animals were anesthetized with isofluorane (2 – 3%), and a mixture of 30% N_2O and 70% O_2 and an osmotic mini-pump (ALZET Osmotic Pumps, Model 2002, 200 μl reservoir volume, 14 days delivery; 0.5 μl/hr release rate; Cupertino, CA) was implanted subcutaneously between the scapular blades. This pump was filled either with saline or Lidocaine 2% and connected by a vinyl tube (PVC 60) to a 28-gauge injector (Plastics One, Roanoke, VA) that was stereotaxically implanted in the medial shell of NAc, which suggested to be hedonic hot spot in the NAc [57], and was contralateral to peripheral nerve injury (ML: + 1; DV: - 7; AP: - 1.7, relative to Bregma). Immediately after the pump insertion, these animals received an SNI injury.

Histology

At the end of the observation period of the animals for Experiment B, each animal was deeply anesthetized (60 mg/kg, nembutal, i.p.) and transcardially perfused with 4% paraformaldehyde. The brains were isolated and processed to determine the placement of cannulae. For this purpose, serial sections (40 μm thickness) were stained with Cresyl Violet stain and screened under the microscope.

Results

Experiment A

In this experiment, we tested the effects of peripheral nerve injury on extent of information sharing between NAc and the rest of the brain, as well as on gene expression in NAc. The experimental design is shown in Fig. 1A. Baseline fMRI scans were conducted in rats 2 days prior to SNI or sham injury. At either 5 days or 28 days post-injury, SNI and sham injury rats were imaged again and sacrificed to assess NAc receptor gene expression. SNI animals showed behavioral signs of persistent neuropathic pain, including tactile allodynia after SNI injury (Fig. 1B). Von Frey 50% withdrawal thresholds of the injured paw in SNI animals, but not sham animals, decreased at Day 5 and persisted at Day 28 (two-way ANOVA, for group effect, $F(2,86) = 15.93$, $P < 0.001$; Fisher LSD post-hoc comparison for both Day 5 and Day 28, $P < 0.001$). No difference in withdrawal thresholds was observed for the contralateral paw in SNI or either paw in sham animals ($F(2,86) = 0.18$, $P = 0.83$).

The NAc core and shell display overlapping but differential functional connections—To identify NAc functional connectivity in healthy conditions, we performed a whole-brain functional connectivity analysis using non-parametric permutation tests on resting-state fMRI scans acquired prior to injury (Day-2). rs-fMRI connectivity was evaluated using a seed-based correlational approach. Resting state analyses detect coherent patterns of brain activity in the resting subject, in the absence of a task, by assessing functional connectivity between a seed region and other target brain areas [33]. Based on histological, track tracing, and physiological characteristics in animals [35], the NAc is divided into two major territories, the core and the shell. Both the NAc core and shell exhibited extensive significant correlations with sensory and motor regions, prefrontal cortical regions, hippocampus, thalamus, and hypothalamus, and both regions showed the strongest functional connections with dorsal striatum (CPu, Caudate/Putamen), sensory cortex (S1/2), motor cortex (M1/2), insula (Ins), cingulate (Cg), as well as the medial (mPFC) and orbital (OFC) prefrontal cortices (Fig. 3B, Table S1 and Table S2).

Despite the large overlap in the NAc core and shell connectivity maps, the core and shell were also characterized by differential functional connectivity strengths (Fig. 3C, Table S3 and Table S4). Specifically, the NAc core showed significantly stronger connectivity to Cg, CPu, Ins, OFC, S1/2 (Table S3), whereas the shell exhibited stronger connectivity to the hippocampus (Hipp), thalamus (Tha), hypothalamus (Hy), and mPFC (Table S4). In addition, the right NAc core showed significantly stronger connectivity to the left NAc core, whereas the right NAc shell showed significantly stronger connectivity to the left NAc shell. This demonstrated the core and shell were characterized by specific functional connections, even with the close proximity of the seeds for functional connectivity analysis.

Reorganization of NAc core and shell functional connections in SNI animals—
Our primary hypothesis was that NAc core and shell are important mediators of chronic pain-like behavior following neuropathic injury, which should be reflected in reorganization in information sharing between NAc and the rest of the brain. To examine changes associated with neuropathic pain, a whole-brain t-test determined group differences between

SNI and sham animals at Day-2, as well as Day5 and Day28. At Day-2 and Day5, no significant difference of functional connectivity between SNI and sham animals was seen (data not shown). At Day28, functional connectivity decreased for contralateral NAc core connectivity to the contralateral CPu, bilateral Ins and S1/2, and for ipsilateral NAc core connectivity to the contralateral Ins, and bilateral S1/2; for contralateral NAc shell connectivity to the bilateral S1/2, and Ins (Fig. 4 and Table S5).

Reduced expression of NAc dopamine type 1a, 2, and kappa-opioid receptors in SNI animals—To evaluate NAc receptor gene expression changes with the transition to neuropathic pain, reverse transcriptase, quantitative PCR (RT-qPCR) was conducted on NAc tissue from SNI and sham animals. To determine the possible lateralization of receptor gene expression changes, contralateral and ipsilateral NAc from each animal were collected and analyzed separately. In order to relate receptor gene expression to temporal aspects of chronification, tissue was collected at Day5 and Day28. Efficiency curves using 10-fold dilutions of NAc cDNA were run to validate primer efficiency (Fig. 5A, B for representative curves). RT-qPCR products were also run on a gel to verify a single product and confirm primer specificity (Fig. 5C). All genes of interest were normalized to the GAPDH reference gene and are shown relative to sham animals. Additionally, the properties of NAc ipsilateral to SNI were quantified relative to the ipsilateral sham NAc, whereas the NAc contralateral to SNI injury was quantified relative to the contralateral sham NAc. As Fig. 5D shows, there were no significant changes in the alpha tubulin to GAPDH ratio at either Day5 or Day28 in contralateral or ipsilateral NAc, thereby validating the stability of GAPDH as a reference gene. This analysis focused on genes that are either of particular interest for NAc function (D1, D2) or for pain regulation (opioids cannabinoid receptors). Our analysis revealed no significant changes in transcript expression at Day5 or Day28 for the cannabinoid receptor 1 (CB1), μ-opioid receptor 1 (MOR1), and serotonin1a receptor (5-HT1a) (data not shown). Interestingly, the κ-opioid receptor (KOR) transcript showed no significant changes at Day5, yet a significant 27% reduction was identified only in contralateral NAc in SNI animals at Day28 (two-way ANOVA, post-hoc Fisher LSD comparison, $P = 0.03$), relative to sham animals (Fig. 5E). Furthermore, the DR1a transcript also showed no significant changes at Day5, but it showed a significant 30% reduction in the contralateral NAc only at Day28 ($P = 0.02$) (Fig. 5F). The DR2 transcript also showed no significant changes at Day5, yet a significant 21% reduction in the contralateral NAc at Day28 was observed ($P = 0.01$) (Fig. 5G). These data demonstrate that peripheral nerve injury induces significant, time dependent changes in the expression of several important genes within the NAc. Moreover, these changes are lateralized, occurring in the NAc contralateral to injury. Although no significant changes were detected in the NAc ipsilateral to injury, there were trends for a reduction in DR1a ($P = 0.12$) and DR2 ($P = 0.11$) receptor gene expression in SNI animals at Day28.

We also observe that the interaction between receptor genes (influence of one receptor on another) shifts in time after SNI. The latter was quantitated by the covariance matrix for receptor gene expression in NAc at Day5 and Day28 in SNI and sham animals, and represented as a receptor- network connectivity graph (Fig. 6). We observed a general upregulation of covariance between the genes examined in SNI animals at Day5, which subsequently (at Day28) subsided to levels comparable to sham animals. Across both groups

and time intervals the expression of DR1a and DR2 (DR1/DR2), and the expression of CB1 and 5-HT1a (CB1/5-HT1a), were positively interrelated within and across contralateral and ipsilateral NAc, whereas these gene pairs were negatively interrelated with each other. If we treat the measured pair-wise correlations as random samples, then we can quantify these general observations. The covariance matrix for DR1a, DR2, both within and across contralateral and ipsilateral NAc (Table S6A) shows a strong group by time interaction ($F(1,20) = 15.2$, $P < 0.001$), with a post-hoc Bonferroni comparison showing significantly higher covariance in SNI animals at Day5 (mean strength = 0.87, S.E.M. = 0.07) in contrast to sham animals at Day5 (mean strength = 0.44, $P < 0.001$). No group differences were identified at Day28 (SNI mean strength = 0.60; sham = 0.74). A similar analysis for the CB1 and 5-HT1a covariance matrix (Table S6B) shows only a time effect ($F(1,20) = 7.5$, $P < 0.01$), with a higher overall covariance strength at Day5 (mean strength = 0.65 with S.E.M. = 0.06), in contrast to Day28 (mean strength = 0.40). We also tested the covariance matrix linking the DR1a/DR2 with the CB1/5HT1a (Table S6C). The covariance matrix was significant for group ($F(1,20) = 26.9$, $P < 10^{-5}$), time ($F(1,20) = 5.1$, $P < 0.03$), and group-by-time interaction ($F(1,20) = 10.4$, $P < 0.005$). Post-hoc Bonferroni comparisons indicated significantly higher negative covariance in SNI animals at Day5 (mean strength = - 0.61, S.E.M. = 0.04), in contrast to sham animals at Day5 (mean strength = - 0.19, $P < 10^{-6}$). Again, no difference between the groups was found at Day28 (SNI mean strength = - 0.33; sham = - 0.24). Thus, we observe that the positive strength of the DR1a/DR2 is elevated, whereas the negative interaction between the DR1a/DR2 and CB1/5-HT1a is enhanced, early after peripheral nerve injury in the SNI animals.

Relating NAc functional connectivity to receptor gene expression and to pain behavior—We performed correlation analyses to explore the longitudinal association between changes in functional connectivity in SNI animals with pain behavior and receptor gene expression. First, functional connectivity of contralateral NAc core to the brain voxels, which was previously identified as decreased in SNI animals and was contralateral to injury, was averaged for this correlation analysis. This contralateral NAc core functional connectivity was significantly different among group and across time (two-way ANOVA, for group-by-time effect, $F(2,77) = 6.31$, $P = 0.014$; Fisher LSD post-hoc comparison on between SNI and sham animals at Day28, $P < 0.001$; difference between SNI animals at Day28 and Day-2, $P = 0.002$) (Fig. 7A bar graph). This functional connectivity (pooling the Day5 and Day28 time points) exhibited a significant negative correlation with DR2 gene expression in SNI animals ($R = - 0.52$, $P = 0.01$), but not in sham animals ($R = - 0.13$, $P = 0.57$), and also showed trends with SNI DR1a ($R = - 0.32$, $P = 0.13$) and KOR ($R = -0.36$, $P = 0.09$, data not shown) gene expression, and was also significantly positively correlated with pain behavior in SNI animals ($R = 0.62$, $P = 0.002$), but not in sham animals ($R = - 0.08$, $P = 0.73$) (Fig. 7A scatter plots). In addition, shell functional connectivity of contralateral NAc to the brain voxels, which were previously identified as decreased in SNI animals and was contralateral to injury, was averaged for this correlation analysis. This contralateral NAc shell functional connectivity was significantly different among group and across time (two-way ANOVA, for group-by-time effect, $F(2,77) = 4.71$, $P = 0.033$; Fisher LSD post-hoc comparison on difference between SNI and sham animals at Day28, $P < 0.001$; difference between SNI animals at Day28 and Day-2, $P = 0.03$) (Fig. 7B bar graph).

This functional connectivity (pooling the Day5 and Day28 time points) approached a borderline of significance of correlation with DR2 gene expression in SNI animals (R = - 0.38, P = 0.08) but not in sham animals (R = - 0.12, P = 0.58), and also showed trends with SNI DR1a (R = - 0.25, P = 0.24) and KOR (R = −0.30, P = 0.16, data not shown) gene expression, but did not correlate with pain behavior in SNI animals (R = 0.24, P = 0.26) and sham animals (R = - 0.02, P = 0.92) (Fig. 7B scatter plots). No correlation was found between functional connectivity and alpha tubulin expression (data not shown). These results indicate that peripheral nerve injury-induced modulation of NAc connectivity in SNI animals is differentially related with changes in DR2 gene expression and to mechanical allodynia.

Experiment B

Continuous lidocaine infusion in NAc decreases mechanical and cold hypersensitivity in SNI animals—There is good evidence that plasticity of the NAc is necessary for the consolidation of appetitive instrumental memories [38]. Appetitive instrumental memory is a form of associative memory. It is the process by which new rewards are learned and acquire their motivational salience. Within this context, the reorganization of NAc functional connectivity observed in SNI animals (Experiment A) can be interpreted as evidence for the involvement of NAc-mediated learning processes in the transition to a neuropathic state. To test this hypothesis directly in a new cohort of animals, we examined the effects of reversibly interrupting neuronal activity of NAc (by a 2-week continuous infusion of lidocaine 2%, started at the time when peripheral nerve injury was inflicted), on the maintenance and temporal evolution of signs for neuropathic pain-like behavior (Fig. 2).

Lidocaine (targeting mainly the contralateral medial shell of NAc (Fig. 8A), which is suggested to be hedonic hot spot in the NAc [57], significantly decreased the magnitude of tactile allodynia during treatment (two-way repeated-measures ANOVA, with time as repeat measure for group effect, $F(1,13) = 7.19$, $P = 0.02$) (Fig. 8B). After cessation of treatment at Day14, lidocaine-infused animals progressively returned to tactile sensitivity levels of saline infused animals. There was no difference between groups for the tactile thresholds of the uninjured paw at any time point (data not shown).

Lidocaine-infused animals also exhibited a decrease in cold allodynia during lidocaine treatment compared with the saline-infused animals (Fig. 8C). Cold allodynia score was significantly lower in lidocaine-infused animals compared to saline-infused animals during the treatment ($F(1,13) = 9.19$, $P = 0.01$).

Discussion

We demonstrate differential functional connectivity of NAc core and shell, in the healthy rat, with cortical and sub-cortical regions. This functional connectivity reorganization was not detected at 5 days but rather 28 days following neuropathic injury, and not in sham animals. Functional connectivity primarily exhibited a long-term reduction in strength of communication between ventral and dorsal striatum and to specific cortical regions. This reduction of functional connectivity is specific to the location of the seed and to the body

side where peripheral nerve injury was inflicted. RT-qPCR complemented the fMRI results by showing that gene expression for multiple receptors decreased at Day 28 only in NAc contralateral to the injury. Furthermore, we also observed upregulation of receptor gene expression covariance early after neuropathic injury. Critically, receptor expression and neuropathic pain-related behavioral outcomes were related to long-term fMRI changes. This is the first study that provides functional and molecular evidence for the reorganization of NAc properties with the transition to neuropathic pain, and demonstrates that disrupting NAc neuronal activity reduces expression of neuropathic pain-related behavior.

In healthy anesthetized animals, fMRI revealed that the NAc core and shell exhibited extensive connectivity to cortical and sub-cortical regions. Whereas the core had significantly stronger connectivity to sensorimotor cortices, insula, cingulate and CPu, the shell exhibited stronger connectivity to hippocampus, thalamus, hypothalamus, and mPFC. Note that due to MRI signal loss and geometric distortions we could not investigate functional connections with the amygdala or with brainstem structures, mainly to ventral tegmentum. To our knowledge these results are the first demonstration of functional connectivity of NAc in the rodent, demonstrating corticostriatal connections and revealing components of the cortico–striato–pallidal–thalamocortical loops [2; 4; 49; 56; 73]. We observed prominent connectivity between NAc and CPu, demonstrating the tight coupling between parts of basal ganglia related to emotional learning [3; 70] with the dorsal aspects involved in more cognitive and motor functions [34; 36]. Significant distinctions were found between NAc core and shell in terms of their relative strengths of connectivity, which is consistent with their functional segregation along emotional salience and motivated behavior [59], their well-established differential connectivity [27; 40; 41; 48], with evidence that the two components respond differentially to aversive stimuli [8], and optogenetic data indicating dense hippocampal inputs to the medial shell of NAc [17]. Importantly, our results point to functional connections between NAc and cortical regions that are important in acute and chronic pain, namely, the hippocampus, thalamus, sensorimotor cortices, cingulate, insula, mPFC, and OFC, suggesting that the striatal dopaminergic system is part of the rearrangement of cortical circuits associated with transition to chronic pain.

An important limitation of this study is the potential influence of anesthesia on reported functional connectivity. Strength of functional connectivity is reduced in the anesthetized compared to conscious animals [47]. However, the spatial pattern of functional connectivity in anesthetized animals seems largely consistent with the pattern observed in awake animals [47]. Still, it is likely that fMRI in awake animals may reveal more extensive changes in functional connectivity in SNI animals. Another limitation is that we intentionally limited the volume and concentration of infused lidocaine to a minimum to insure specificity of obtained results. It is likely that the procedure only impacted a limited proportion of NAc, especially core, neurons, and that disruption of more NAc neurons would result in bigger reductions in neuropathic pain behavior.

The NAc receptor inter-relationships were upregulated in SNI animals at Day5, both within the DR1a/DR2 pair, and across the DR1a/DR2 and CB1/5-HT1a pairs. These results suggest enhanced dopamine activity within the NAc and VTA reverberating loops. Thus, these results are the earliest signal we observe in NAc that differentiate between SNI and sham

animals and which imply an enhanced mesolimbic-learning state. Following 28 days of neuropathic pain, when expression levels of DR1a, DR2 and KOR in NAc contralateral to SNI injury are decreased and NAc functional connectivity is also decreased, the receptor inter-relationships seem to return to basal levels, yet with a distinct pattern for SNI. It was surprising to see a tight correlation between DR1a and DR2 expression, given that they comprise two parallel NAc transmission pathways: DR1a expression defines the striatonigral neurons in the direct pathway containing dynorphin, the endogenous ligand for KOR; whereas DR2 are expressed on neurons that comprise the striatopallidal indirect pathway [2; 25; 30; 32; 58]. The direct and indirect pathways are associated with positive hedonic and aversion/negative affect, respectively [15; 52; 57; 58]. Recent studies indicate that activation of DR1 and inactivation of DR2 postsynaptically control reward learning and aversive learning, respectively, in a pathway-specific manner [39]. If we define transition to neuropathic pain as a state of enhanced aversive learning, then we expect to observe changes in the expression of DR2. Indeed, 28 days after injury, we in fact observe down regulation of DR1a, DR2 and KOR. Furthermore, given that only DR2 expression correlated with functional connectivity changes, our data are consistent with the role of aversive-learning circuitry in neuropathic pain.

Numerous studies reinforce the notion that levels of dopamine neurotransmission influence striatal BOLD activity; for example, the administration of D-amphetamine, dopamine re-uptake inhibitors, and DR1a or DR2 antagonists all modulate striatal BOLD activity [21; 28]. Our evidence relating NAc functional connectivity to DR2 expression is consistent with these observations and with previous work showing that 1) components of NAc functional connectivity and receptor gene expression were dominantly reduced contralaterally at Day28, 2) NAc functional connectivity was related to SNI pain behavior and to DR2 expression, and 3) the disruption of NAc neural activity (chronic perfusion of a DR agonist) in NAc attenuates neuropathic behavior in SNI animals [60], which is also consistent with our evidence of lidocaine infusion in NAc reducing SNI neuropathic behaviors.

The NAc has been a central site for studying reward and drug reinforcement and for the transition between drug use as a reward and as an addictive habit [45; 67]. In fact, the reorganization we describe here for neuropathic pain has many parallels to processes implicated in addictive behavior. In humans, addicted states are associated with decreased DR2 expression in the striatum [69]. Similarly, with sustained neuropathic pain, we observe decreased DR2 expression in NAc. In rodent models of addiction, decreased dopamine release in the ventral striatum is coupled with increased dopamine release in dorsal striatum [72]. Similarly, we observed a decreased synchronization of resting fMRI activity between ventral and dorsal striatum, and this de-synchronization was associated with DR2 expression in NAc. These parallels are suggestive that brain learning circuitry perpetuate or aid in the persistence of pain perception by rendering the perception more habitual, a hypothesis derived from current theories of addiction as a shift of cued behavior into a habitual state [14]; as such, chronic pain seems to highjack brain learning circuitry in a manner similar to addictive behavior. The extent to which addiction to pain shares brain emotional learning mechanisms with those for rewarding drugs remains to be determined, and raises the question as to whether predisposition to chronic pain is part of a generalized predisposition to addictive behavior, or whether it is a specific addictive trait for aversive conditions.

Supplementary Material

Refer to Web version on PubMed Central for supplementary material.

Acknowledgments

References and Notes

1. Abi-Dargham A, Rodenhiser J, Printz D, Zea-Ponce Y, Gil R, Kegeles LS, Weiss R, Cooper TB, Mann JJ, Van Heertum RL, Gorman JM, Laruelle M. Increased baseline occupancy of D2 receptors by dopamine in schizophrenia. Proc Natl Acad Sci U S A. 2000; 97(14):8104–8109. [PubMed: 10884434]

2. Alexander GE, Crutcher MD. Functional architecture of basal ganglia circuits: neural substrates of parallel processing. Trends Neurosci. 1990; 13(7):266–271. [PubMed: 1695401]

3. Alexander GE, Crutcher MD, DeLong MR. Basal ganglia-thalamocortical circuits: parallel substrates for motor, oculomotor, "prefrontal" and "limbic" functions. Prog Brain Res. 1990; 85:119–146. [PubMed: 2094891]

4. Alexander GE, DeLong MR, Strick PL. Parallel organization of functionally segregated circuits linking basal ganglia and cortex. Annu Rev Neurosci. 1986; 9:357–381. [PubMed: 3085570]

5. Ambroggi F, Ishikawa A, Fields HL, Nicola SM. Basolateral amygdala neurons facilitate reward-seeking behavior by exciting nucleus accumbens neurons. Neuron. 2008; 59(4):648–661. [PubMed: 18760700]

6. Ansah OB, Leite-Almeida H, Wei H, Pertovaara A. Striatal dopamine D2 receptors attenuate neuropathic hypersensitivity in the rat. Exp Neurol. 2007; 205(2):536–546. [PubMed: 17451685]

7. Apkarian AV. Pain perception in relation to emotional learning. CurrOpinNeurobiol. 2008; 18(4): 464–468.

8. Badrinarayan A, Wescott SA, Vander Weele CM, Saunders BT, Couturier BE, Maren S, Aragona BJ. Aversive stimuli differentially modulate real-time dopamine transmission dynamics within the nucleus accumbens core and shell. J Neurosci. 2012; 32(45):15779–15790. [PubMed: 23136417]

9. Baliki MN, Geha PY, Fields HL, Apkarian AV. Predicting Value of Pain and Analgesia: Nucleus Accumbens Response to Noxious Stimuli Changes in the Presence of Chronic Pain. Neuron. 2010; 66(1):149–160. [PubMed: 20399736]

10. Baliki MN, Petre B, Torbey S, Herrmann KM, Huang L, Schnitzer TJ, Fields HL, Apkarian AV. Corticostriatal functional connectivity predicts transition to chronic back pain. Nat Neurosci. 2012; 15(8):1117–1119. [PubMed: 22751038]

11. Bassareo V, De Luca MA, Di Chiara G. Differential Expression of Motivational Stimulus Properties by Dopamine in Nucleus Accumbens Shell versus Core and Prefrontal Cortex. J Neurosci. 2002; 22(11):4709–4719. [PubMed: 12040078]

12. Becerra L, Borsook D. Signal valence in the nucleus accumbens to pain onset and offset. EurJPain. 2008; 12(7):866–869.

13. Becerra L, Breiter HC, Wise R, Gonzalez RG, Borsook D. Reward circuitry activation by noxious thermal stimuli. Neuron. 2001; 32(5):927–946. [PubMed: 11738036]

14. Belin D, Jonkman S, Dickinson A, Robbins TW, Everitt BJ. Parallel and interactive learning processes within the basal ganglia: relevance for the understanding of addiction. Behav Brain Res. 2009; 199(1):89–102. [PubMed: 18950658]

15. Bozarth MA, Wise RA. Intracranial self-administration of morphine into the ventral tegmental area in rats. Life sciences. 1981; 28(5):551–555. [PubMed: 7207031]

16. Brischoux F, Chakraborty S, Brierley DI, Ungless MA. Phasic excitation of dopamine neurons in ventral VTA by noxious stimuli. Proceedings of the National Academy of Sciences of the United States of America. 2009; 106(12):4894–4899. [PubMed: 19261850]

17. Britt JP, Benalioud F, McDevitt RA, Stuber GD, Wise RA, Bonci A. Synaptic and behavioral profile of multiple glutamatergic inputs to the nucleus accumbens. Neuron. 2012; 76(4):790–803. [PubMed: 23177963]

18. Bustin SA, Beaulieu JF, Huggett J, Jaggi R, Kibenge FS, Olsvik PA, Penning LC, Toegel S. MIQE precis: Practical implementation of minimum standard guidelines for fluorescence-based quantitative real-time PCR experiments. BMC molecular biology. 2010; 11:74. [PubMed: 20858237]

19. Carlezon WA Jr, Thomas MJ. Biological substrates of reward and aversion: a nucleus accumbens activity hypothesis. Neuropharmacology. 2009; 56(Suppl 1):122–132. [PubMed: 18675281]

20. Chaplan SR, Bach FW, Pogrel JW, Chung JM, Yaksh TL. Quantitative assessment of tactile allodynia in the rat paw. JNeurosciMethods. 1994; 53(1):55–63.

21. Chen YC, Galpern WR, Brownell AL, Matthews RT, Bogdanov M, Isacson O, Keltner JR, Beal MF, Rosen BR, Jenkins BG. Detection of dopaminergic neurotransmitter activity using pharmacologic MRI: correlation with PET, microdialysis, and behavioral data. Magn Reson Med. 1997; 38(3):389–398. [PubMed: 9339439]

22. Choi Y, Yoon YW, Na HS, Kim SH, Chung JM. Behavioral signs of ongoing pain and cold allodynia in a rat model of neuropathic pain. Pain. 1994; 59(3):369–376. [PubMed: 7708411]

23. Coizet V, Dommett EJ, Redgrave P, Overton PG. Nociceptive responses of midbrain dopaminergic neurones are modulated by the superior colliculus in the rat. Neuroscience. 2006; 139(4):1479–1493. [PubMed: 16516396]

24. Decosterd I, Woolf CJ. Spared nerve injury: an animal model of persistent peripheral neuropathic pain. Pain. 2000; 87(2):149–158. [PubMed: 10924808]

25. Deniau JM, Mailly P, Maurice N, Charpier S. The pars reticulata of the substantia nigra: a window to basal ganglia output. Prog Brain Res. 2007; 160:151–172. [PubMed: 17499113]

26. Dennis SG, Melzack R. Effects of cholinergic and dopaminergic agents on pain and morphine analgesia measured by three pain tests. Exp Neurol. 1983; 81(1):167–176. [PubMed: 6861945]

27. Di Chiara G. Nucleus accumbens shell and core dopamine: differential role in behavior and addiction. Behav Brain Res. 2002; 137(1–2):75–114. [PubMed: 12445717]

28. Dixon AL, Prior M, Morris PM, Shah YB, Joseph MH, Young AMJ. Dopamine antagonist modulation of amphetamine response as detected using pharmacological MRI. Neuropharmacology. 2005; 48(2):236–245. [PubMed: 15695162]

29. Franklin KB. Analgesia and the neural substrate of reward. Neuroscience and biobehavioral reviews. 1989; 13(2–3):149–154. [PubMed: 2682401]

30. Gerfen CR, Engber TM, Mahan LC, Susel Z, Chase TN, Monsma FJ Jr, Sibley DR. D1 and D2 dopamine receptor-regulated gene expression of striatonigral and striatopallidal neurons. Science. 1990; 250(4986):1429–1432. [PubMed: 2147780]

31. Goeders NE, Smith JE. Cortical dopaminergic involvement in cocaine reinforcement. Science. 1983; 221(4612):773–775. [PubMed: 6879176]

32. Graybiel AM. The basal ganglia. Curr Biol. 2000; 10(14):R509–R511. [PubMed: 10899013]

33. Gusnard DA, Raichle ME. Searching for a baseline: functional imaging and the resting human brain. NatRevNeurosci. 2001; 2(10):685–694.

34. Haber SN. The primate basal ganglia: parallel and integrative networks. J Chem Neuroanat. 2003; 26(4):317–330. [PubMed: 14729134]

35. Haber, SN. Neuroanatomy of Reward: A View from the Ventral Striatum. In: Gottfried, JA., editor. Neurobiology of Sensation and Reward. Boca Raton (FL): 2011.

36. Haber SN, Fudge JL, McFarland NR. Striatonigrostriatal pathways in primates form an ascending spiral from the shell to the dorsolateral striatum. J Neurosci. 2000; 20(6):2369–2382. [PubMed: 10704511]

37. Hagelberg N, Forssell H, Aalto S, Rinne JO, Scheinin H, Taiminen T, Nagren K, Eskola O, Jaaskelainen SK. Altered dopamine D2 receptor binding in atypical facial pain. Pain. 2003; 106(1–):43–48. [PubMed: 14581109]

38. Hernandez PJ, Sadeghian K, Kelley AE. Early consolidation of instrumental learning requires protein synthesis in the nucleus accumbens. Nat Neurosci. 2002; 5(12):1327–1331. [PubMed: 12426572]

39. Hikida T, Yawata S, Yamaguchi T, Danjo T, Sasaoka T, Wang Y, Nakanishi S. Pathway-specific modulation of nucleus accumbens in reward and aversive behavior via selective transmitter receptors. Proc Natl Acad Sci U S A. 2013; 110(1):342–347. [PubMed: 23248274]

40. Ikemoto S. Dopamine reward circuitry: two projection systems from the ventral midbrain to the nucleus accumbens-olfactory tubercle complex. Brain Res Rev. 2007; 56(1):27–78. [PubMed: 17574681]

41. Ito R, Hayen A. Opposing roles of nucleus accumbens core and shell dopamine in the modulation of limbic information processing. J Neurosci. 2011; 31(16):6001–6007. [PubMed: 21508225]

42. Jarcho JM, Mayer EA, Jiang ZK, Feier NA, London ED. Pain, affective symptoms, and cognitive deficits in patients with cerebral dopamine dysfunction. Pain. 2012; 153(4):744–754. [PubMed: 22386471]

43. Joshua M, Adler A, Mitelman R, Vaadia E, Bergman H. Midbrain dopaminergic neurons and striatal cholinergic interneurons encode the difference between reward and aversive events at different epochs of probabilistic classical conditioning trials. JNeurosci. 2008; 28(45):11673–11684. [PubMed: 18987203]

44. Kalivas PW, Duffy P. Selective activation of dopamine transmission in the shell of the nucleus accumbens by stress. Brain Res. 1995; 675(1–2):325–328. [PubMed: 7796146]

45. Kalivas PW, Volkow N, Seamans J. Unmanageable motivation in addiction: a pathology in prefrontal-accumbens glutamate transmission. Neuron. 2005; 45(5):647–650. [PubMed: 15748840]

46. Levy I, Snell J, Nelson AJ, Rustichini A, Glimcher PW. Neural representation of subjective value under risk and ambiguity. J Neurophysiol. 2010; 103(2):1036–1047. [PubMed: 20032238]

47. Liang Z, King J, Zhang N. Intrinsic organization of the anesthetized brain. J Neurosci. 2012; 32(30):10183–10191. [PubMed: 22836253]

48. Loriaux AL, Roitman JD, Roitman MF. Nucleus accumbens shell, but not core, tracks motivational value of salt. J Neurophysiol. 2011; 106(3):1537–1544. [PubMed: 21697439]

49. Luscher C, Malenka RC. Drug-evoked synaptic plasticity in addiction: from molecular changes to circuit remodeling. Neuron. 2011; 69(4):650–663. [PubMed: 21338877]

50. Maeda H, Mogenson GJ. Effects of peripheral stimulation on the activity of neurons in the ventral tegmental area, substantia nigra and midbrain reticular formation of rats. Brain Res Bull. 1982; 8(1):7–14. [PubMed: 7055735]

51. McCutcheon JE, Ebner SR, Loriaux AL, Roitman MF. Encoding of aversion by dopamine and the nucleus accumbens. Front Neurosci. 2012; 6:137. [PubMed: 23055953]

52. Mucha RF, Herz A. Motivational properties of kappa and mu opioid receptor agonists studied with place and taste preference conditioning. Psychopharmacology (Berl). 1985; 86(3):274–280. [PubMed: 2994144]

53. Narita M, Suzuki M, Imai S, Narita M, Ozaki S, Kishimoto Y, Oe K, Yajima Y, Yamazaki M, Suzuki T. Molecular mechanism of changes in the morphine-induced pharmacological actions under chronic pain-like state: suppression of dopaminergic transmission in the brain. Life sciences. 2004; 74(21):2655–2673. [PubMed: 15041447]

54. Navratilova E, Xie JY, Okun A, Qu C, Eyde N, Ci S, Ossipov MH, King T, Fields HL, Porreca F. Pain relief produces negative reinforcement through activation of mesolimbic reward-valuation circuitry. Proc Natl Acad Sci U S A. 2012; 109(50):20709–20713. [PubMed: 23184995]

55. Nichols TE, Holmes AP. Nonparametric permutation tests for functional neuroimaging: a primer with examples. HumBrain Mapp. 2002; 15(1):1–25.

56. O'Donnell P, Lavin A, Enquist LW, Grace AA, Card JP. Interconnected parallel circuits between rat nucleus accumbens and thalamus revealed by retrograde transynaptic transport of pseudorabies virus. J Neurosci. 1997; 17(6):2143–2167. [PubMed: 9045740]

57. Pecina S, Berridge KC. Hedonic hot spot in nucleus accumbens shell: where do mu-opioids cause increased hedonic impact of sweetness? J Neurosci. 2005; 25(50):11777–11786. [PubMed: 16354936]

58. Pfeiffer A, Brantl V, Herz A, Emrich HM. Psychotomimesis mediated by kappa opiate receptors. Science. 1986; 233(4765):774–776. [PubMed: 3016896]

59. Reynolds SM, Berridge KC. Positive and negative motivation in nucleus accumbens shell: bivalent rostrocaudal gradients for GABA-elicited eating, taste "liking"/"disliking" reactions, place preference/avoidance, and fear. J Neurosci. 2002; 22(16):7308–7320. [PubMed: 12177226]

60. Sarkis R, Saade N, Atweh S, Jabbur S, Al-Amin H. Chronic dizocilpine or apomorphine and development of neuropathy in two rat models I: behavioral effects and role of nucleus accumbens. Exp Neurol. 2011; 228(1):19–29. [PubMed: 21146525]

61. Schmittgen TD, Livak KJ. Analyzing real-time PCR data by the comparative C(T) method. Nature protocols. 2008; 3(6):1101–1108. [PubMed: 18546601]

62. Schultz W, Romo R. Responses of nigrostriatal dopamine neurons to high-intensity somatosensory stimulation in the anesthetized monkey. J Neurophysiol. 1987; 57(1):201–217. [PubMed: 3559672]

63. Schwarz AJ, Danckaert A, Reese T, Gozzi A, Paxinos G, Watson C, Merlo-Pich EV, Bifone A. A stereotaxic MRI template set for the rat brain with tissue class distribution maps and co-registered anatomical atlas: application to pharmacological MRI. Neuroimage. 2006; 32(2):538–550. [PubMed: 16784876]

64. Scott DJ, Heitzeg MM, Koeppe RA, Stohler CS, Zubieta JK. Variations in the human pain stress experience mediated by ventral and dorsal basal ganglia dopamine activity. J Neurosci. 2006; 26(42):10789–10795. [PubMed: 17050717]

65. Seymour B, O'Doherty JP, Koltzenburg M, Wiech K, Frackowiak R, Friston K, Dolan R. Opponent appetitive-aversive neural processes underlie predictive learning of pain relief. NatNeurosci. 2005; 8(9):1234–1240.

66. Smith SM, Nichols TE. Threshold-free cluster enhancement: addressing problems of smoothing, threshold dependence and localisation in cluster inference. Neuroimage. 2009; 44(1):83–98. [PubMed: 18501637]

67. Taha SA, Fields HL. Inhibitions of nucleus accumbens neurons encode a gating signal for reward-directed behavior. J Neurosci. 2006; 26(1):217–222. [PubMed: 16399690]

68. Ungless MA, Magill PJ, Bolam JP. Uniform inhibition of dopamine neurons in the ventral tegmental area by aversive stimuli. Science. 2004; 303(5666):2040–2042. [PubMed: 15044807]

69. Volkow ND, Fowler JS, Wang GJ, Swanson JM, Telang F. Dopamine in drug abuse and addiction: results of imaging studies and treatment implications. Arch Neurol. 2007; 64(11):1575–1579. [PubMed: 17998440]

70. Voorn P, Vanderschuren LJ, Groenewegen HJ, Robbins TW, Pennartz CM. Putting a spin on the dorsal-ventral divide of the striatum. Trends Neurosci. 2004; 27(8):468–474. [PubMed: 15271494]

71. Wasner G, Deuschl G. Pains in Parkinson disease--many syndromes under one umbrella. Nature reviews Neurology. 2012; 8(5):284–294. [PubMed: 22508236]

72. Willuhn I, Burgeno LM, Everitt BJ, Phillips PE. Hierarchical recruitment of phasic dopamine signaling in the striatum during the progression of cocaine use. Proc Natl Acad Sci U S A. 2012; 109(50):20703–20708. [PubMed: 23184975]

73. Zahm DS, Brog JS. On the significance of subterritories in the "accumbens" part of the rat ventral striatum. Neuroscience. 1992; 50(4):751–767. [PubMed: 1448200]
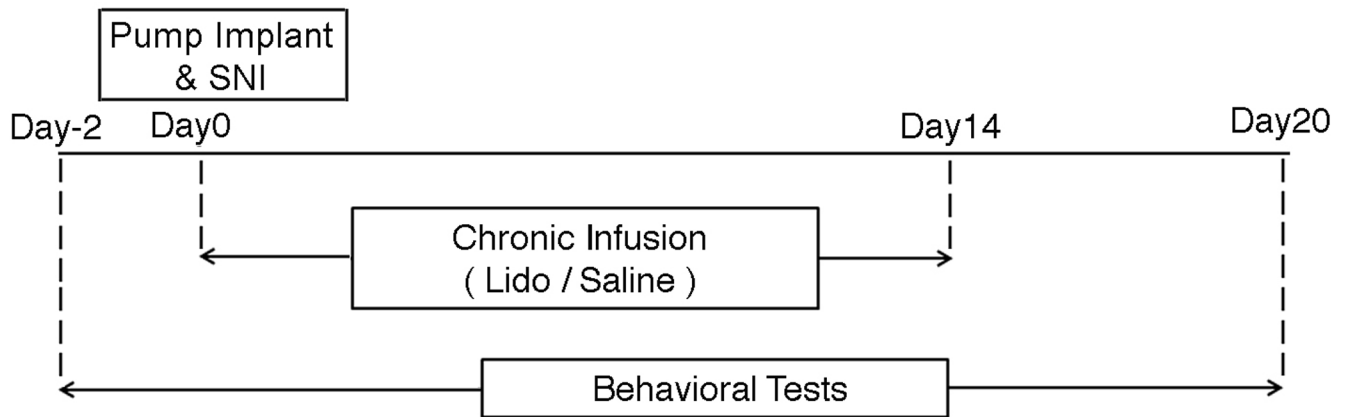
Experiment A

A
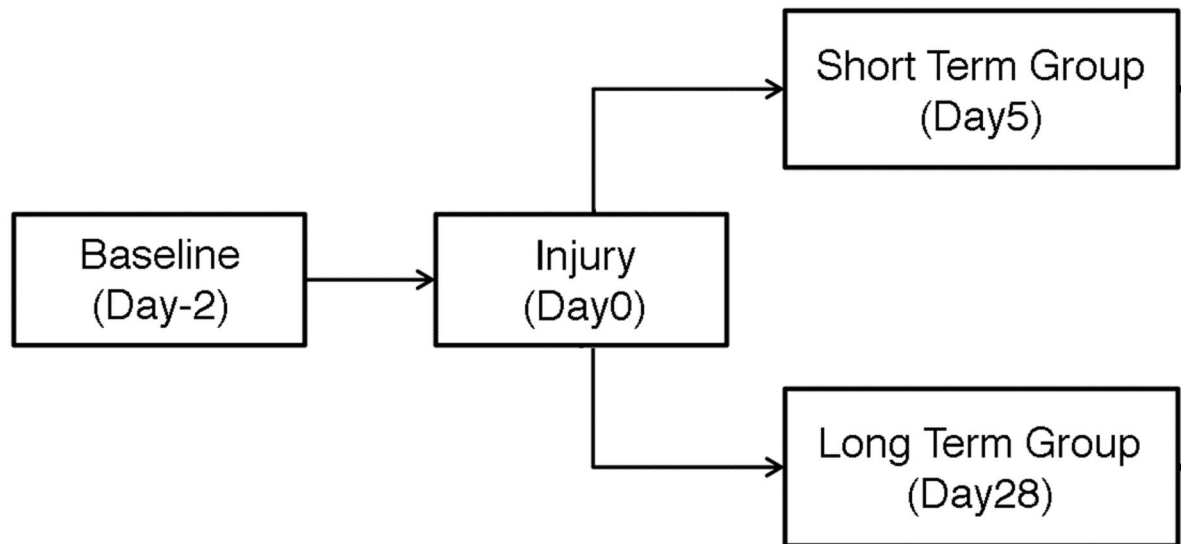
B
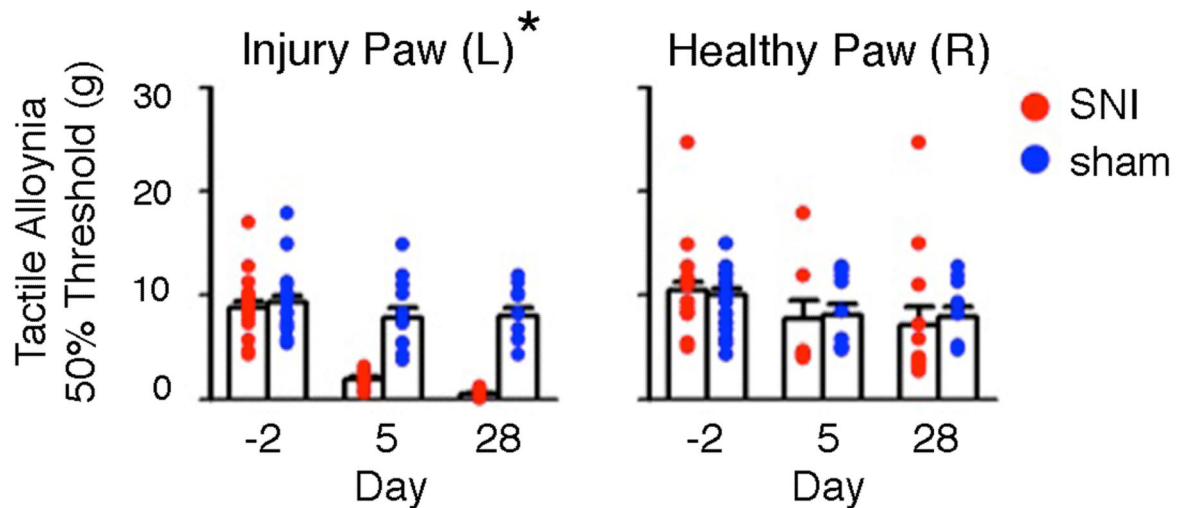
Fig. 1. Paradigm for Experiment A, and tactile sensitivity changes following peripheral nerve injury

(**A**) MRI scans at baseline were acquired at Day-2. Animals were randomly selected to receive either SNI or sham injury (Day 0) and were divided into the Short Term or Long Term group. First, at Day5 (Short Term Group, Day5) both SNI and sham animals underwent MRI, followed by extraction of NAc tissue for receptor gene expression analysis. Similarly, at Day28 (Long Term Group, Day28) SNI and sham animals underwent MRI and also extraction of NAc tissue. MRI at Day5 was performed in: SNI=10, sham=12 animals; MRI at Day28 was done in: SNI=13, sham=11 animals. RT-qPCR at Day5: was done in

SNI=14, sham=13 animals; while at Day28 it was done in: SNI=14, sham=12 animals. Because physiological recording was used for fMRI data pre-processing, rats with incomplete physiological recordings during the scans were excluded from the fMRI study; however these rats were still included in the receptor gene expression analysis. Tests for tactile allodynia were performed one day prior to each MRI scan. **(B)** Tactile allodynia in the injury paw of SNI animals were persistent over time. No change in tactile threshold was observed in the healthy paw of both SNI and sham animals. Tactile thresholds are shown for animals used in MRI experiment illustrated for Experiment A. *P < 0.05.

Experiment B

Fig. 2. Paradigm of Experiment B
In a different group of animals from Experiment A, NAc activity, contralateral to peripheral nerve injury, was disrupted either by infusing Lidocaine 2% (n=8) or saline (n=7), for 14 days using implanted mini pumps in the NAc. The mini pumps were implanted at the same surgical procedure when SNI injury was induced. Behavioral tests for tactile and cold allodynia were assessed twice at Day-2 as well as on Day4, Day7, Day10, Day14, Day17 and Day20.
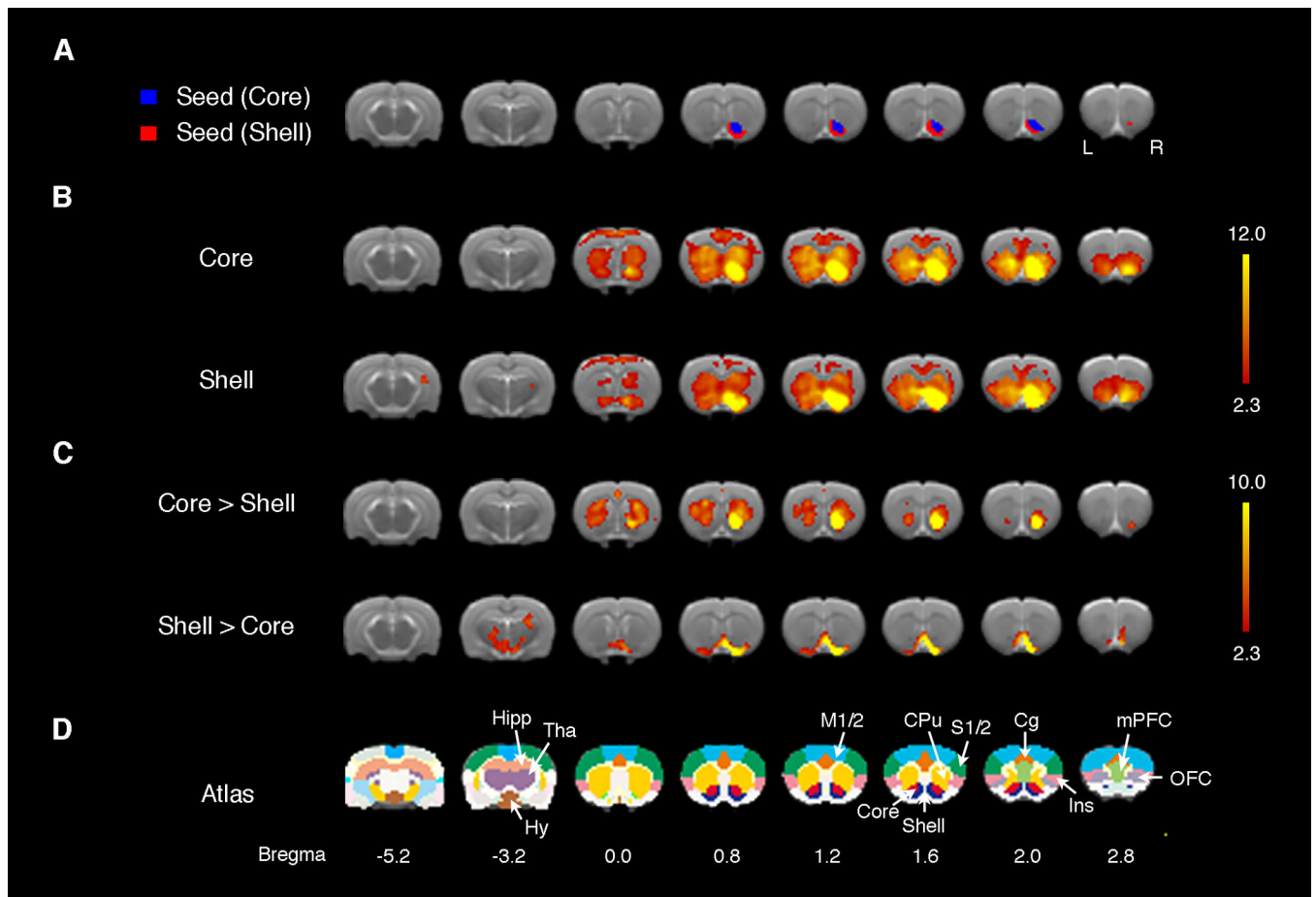
Fig. 3. Functional connectivity of NAc core and shell in healthy animals
(**A**) The core and shell subdivisions of NAc are illustrated, as location of seeds used to study functional connectivity of each subdivision. (**B**) Group-averaged functional connectivity maps from NAc core and shell are shown in indicated rows, for resting state fMRI (rs-fMRI) when animals were healthy (collected at Day-2). Group-average was across all animals (n = 36 rats). NAc core and shell exhibited strongest functional connectivity to CPu, S1/2, M1/2, Cg, Ins, mPFC and OFC, see Table S1 and Table S2 (one-sample T-test, P < 0.05, family-wise error (FWE)-corrected). (**C**) NAc core and shell show preferential functional connectivity. The core (core > shell contrast) showed significantly stronger connectivity to CPu, S1/2, Cg, Ins, and OFC; while the shell (shell > core contrast) exhibited significantly higher connectivity to parts of Hipp, Tha, Hy, and mPFC, see Table 4 and Table 5 (paired T-test, P < 0.05, FWE-corrected). (**D**) Brain atlas slices highlighting anatomical borders. Columns of axial slices, shown in B-D, correspond to each other (distance from Bregma in mm indicated at bottom). Functional connectivity maps are for seeds placed in the right side of the brain. Color bars represent range of t-values. Abbreviation: Cg = cingulate cortex, CPu = caudate/putamen, Hipp = hippocampus, Hy = hypothalamus, Tha = thalamus, S1/2 = primary and secondary S1/2sensory cortices, M1/2 = primary and secondary motor cortices, Ins = insular cortex, mPFC = medial prefrontal cortex, OFC = orbital frontal cortex, R = right, L = left side of the brain.
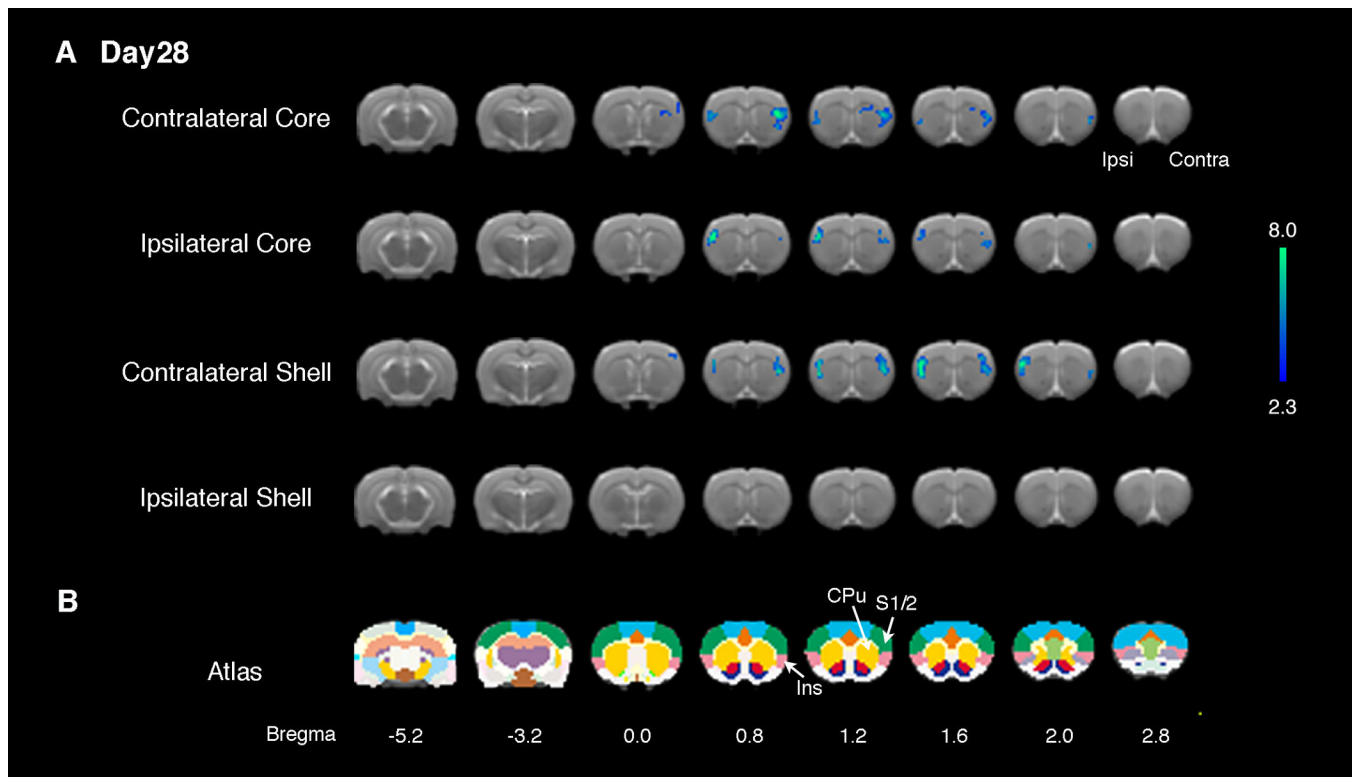
**Fig. 4. Differences in functional connectivity of NAc core and shell between SNI and sham animals**

Between groups functional connectivity contrasts (SNI vs. sham, cross-sectional unpaired two-sample t-tests) were significantly different at Day28, illustrated for the four seed placements indicated. No significant difference was seen at Day5. (**A**) At Day28, functional connectivity decrease was seen. For contralateral NAc core, connectivity decreased to contralateral CPu, bilateral Ins and S1/2, and for ipsilateral NAc core connectivity to the contralateral Ins, and bilateral S1/2; while for contralateral NAc shell, connectivity decreased to contralateral Ins, and bilateral S1/2, see Table S3 and Table S4. All contrasts were thresholded at P < 0.05, FWE-corrected. Color bars represent range of t-values. (**B**) Rat atlas slices corresponding to each column above are shown.
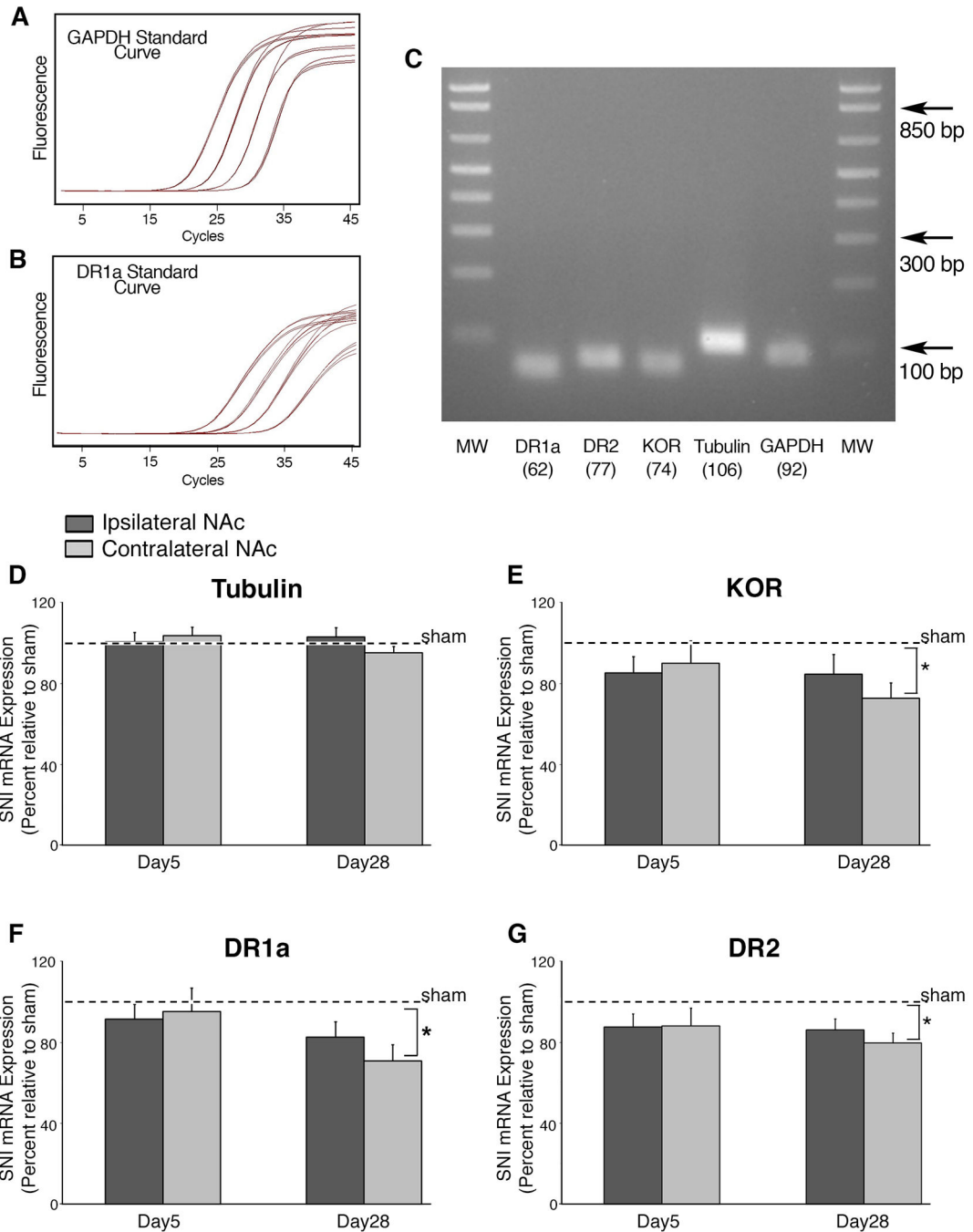
Fig. 5. The Expression of DR1a, DR2, and KOR transcripts are reduced in the NAc contralateral to peripheral nerve injury in SNI animals

(**A**) Validation of GAPDH primers using dilutions of input NAc cDNA over 4 orders of magnitude. The almost perfect doubling of PCR product with each cycle validates this primer pair. (**B**) Representative efficiency curve showing DR1a amplification comprising dilutions over 4 orders of magnitude. (**C**) RT-qPCR products run on a 1.8% agarose gel demonstrate a single amplification product for each gene of interest. (**D**) Relative abundance for genes of interest in the NAc of SNI animals are shown, the ipsilateral SNI is normalized

to the ipsilateral sham, while the contralateral SNI is normalized to the contralateral sham at Day5 and Day 28. Dotted line represents sham levels. For each sample, the gene of interest is normalized to the reference gene GAPDH. Alpha tubulin transcripts, when normalized to GAPDH, showed no significant changes in contralateral or ipsilateral NAc at Day5 and Day28, and validate GAPDH as a stable reference gene. (**E**) KOR transcript showed no significant changes between SNI and sham animals at Day5; however at Day28 a significant (P = 0.03), 27% reduction of transcript is found in the contralateral NAc only. (**F**) DR1a transcript showed no significant changes between SNI and sham animals at Day5, but at Day28 a significant (P = 0.02), 30% reduction is found in the contralateral NAc only. (**G**) DR2 transcript showed no significant changes between SNI and sham animals at Day5, but at Day28 a significant (P = 0.01), 21% reduction was found also in the contralateral NAc. No significant changes were found at any timepoint for the MOR, CB1, and 5-HT1a receptors (data not shown). Abbreviations: KOR = kappa-opioid receptor, MOR= μ-opioid receptor, DR1a = dopamine type 1a receptor, DR2 = dopamine type 2 receptor, CB1 = cannabinoid receptor 1, 5-HT1a = serotonin1a receptor, Tubulin = alpha tubulin, GAPDH = glyceraldehyde-3-phosphate dehydrogenase, and MW = molecular weight. * P < 0.05. (Normalized to GAPDH numbers for qPCR: DR1a: SNI Day5-Ipsi 0.1072, Day5-Contra 0.0991, sham Day5-Ipsi 0.1172, Day5-Contra 0.1040, SNI Day28-Ipsi 0.1255, Day28-Contra 0.0889, sham Day28-Ipsi 0.1520, Day28-Contra 0.1479. DR2: SNI Day5-Ipsi 0.0785, Day5-Contra 0.0720, sham Day5-Ipsi 0.0901, Day5-Contra 0.0820, SNI Day28-Ipsi 0.0961, Day28-Contra 0.0889, sham Day28-Ipsi 0.1129, Day28-Contra 0.1122. KOR: SNI Day5-Ipsi 0.0111, Day5-Contra 0.0106, sham Day5-Ipsi 0.0130, Day5-Contra 0.0188, SNI Day28-Ipsi 0.0154, Day28-Contra 0.0136, sham Day28-Ipsi 0.0182, Day28-Contra 0.0187. Tubulin: SNI Day5-Ipsi 0.3740, Day5-Contra 0.3750, sham Day5-Ipsi 0.3786, Day5-Contra 0.3620, SNI Day28-Ipsi 0.4650, Day28-Contra 0.4410, sham Day28-Ipsi 0.4533, Day28-Contra 0.4636.)
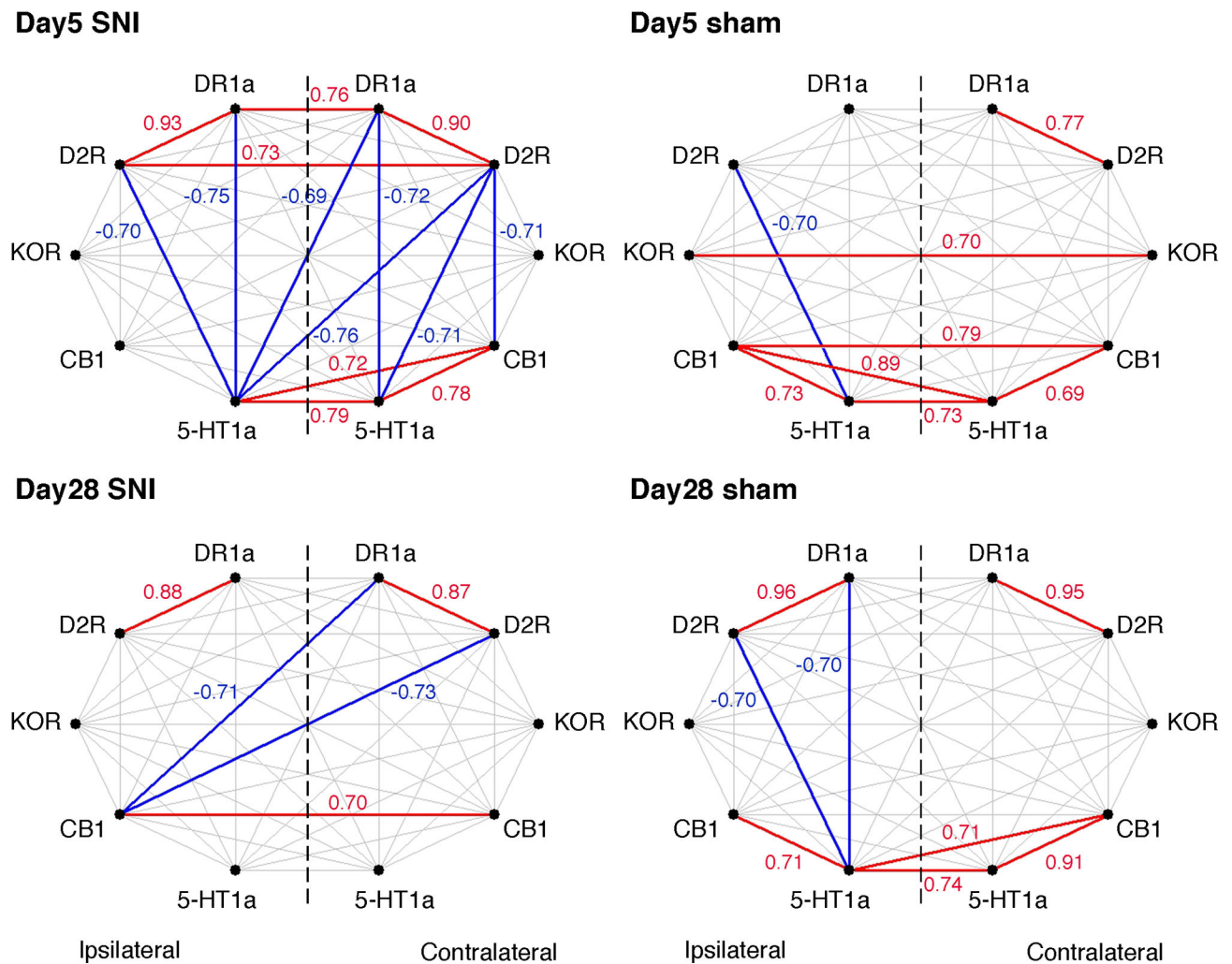
Fig. 6. Gene expression covariance as a function of injury type and time from injury

Correlations between contralateral and ipsilateral NAc gene transcripts for five receptors (DR1a, DR2, KOR, CB1, and 5-HT1a), at a threshold of P < 0.01, are indicated in red (positive) and blue (negative) in a network graph representation. We observe a general upregulation of covariance between the genes examined in SNI animals at Day5, which subsequently subsides to a new state at Day28.
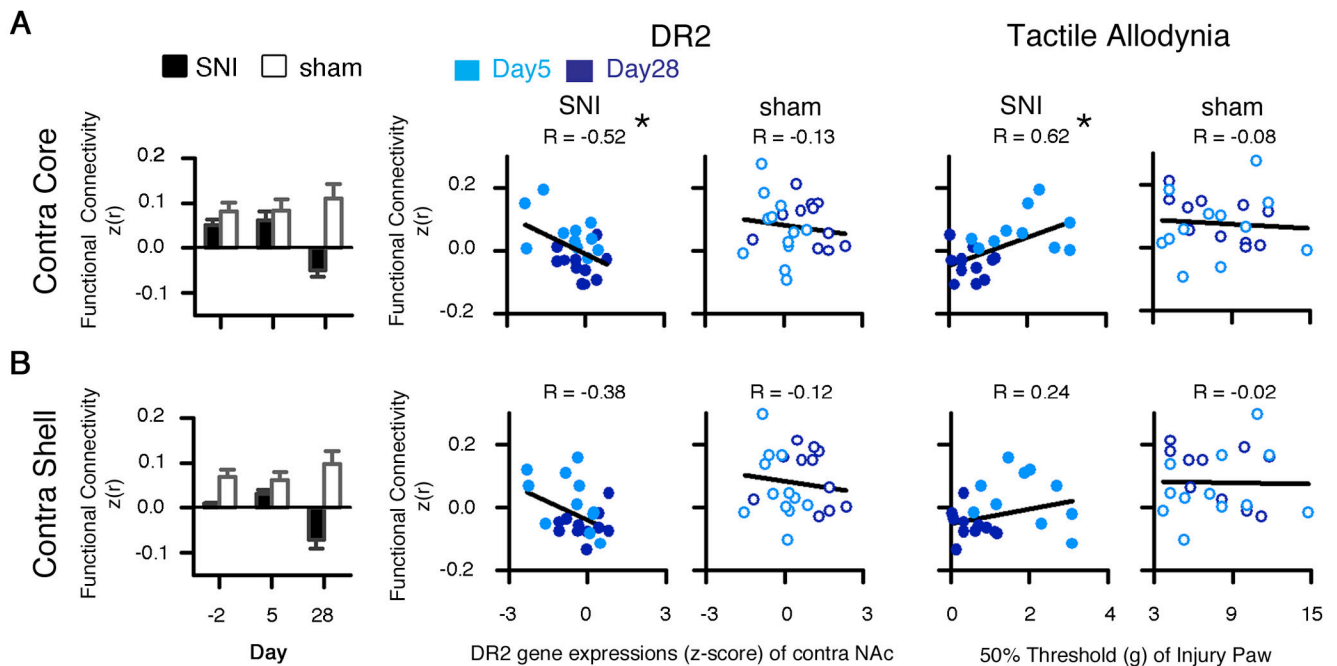
Fig. 7. In SNI animals, decreased NAc functional connectivity correlates with DR2 receptor gene expression and with tactile allodynia

(**A**) Bar graph shows functional connectivity between NAc core contralateral to injury with all of voxels showing significant change and contralateral to injury, while scatter plots show correlations between functional connectivity with DR2 gene expression, and with tactile allodynia for SNI and sham animals. (**B**) Bar graph shows the functional connectivity of NAc shell contralateral to injury with all of voxels showing significant change and contralateral to injury, while scatter plots show the relationship of functional connectivity and DR2 gene expressions. Functional connectivity is expressed in Fisher's z transformed correlation coefficients (z(r)), while DR2 receptor expression is expressed in z-scores. Data points for correlation analysis were pooled from animals from Day5 and Day28. Abbreviation: R = canonical correlation coefficient. #P < 0.05 (post-hoc). *P < 0.05 (correlation).
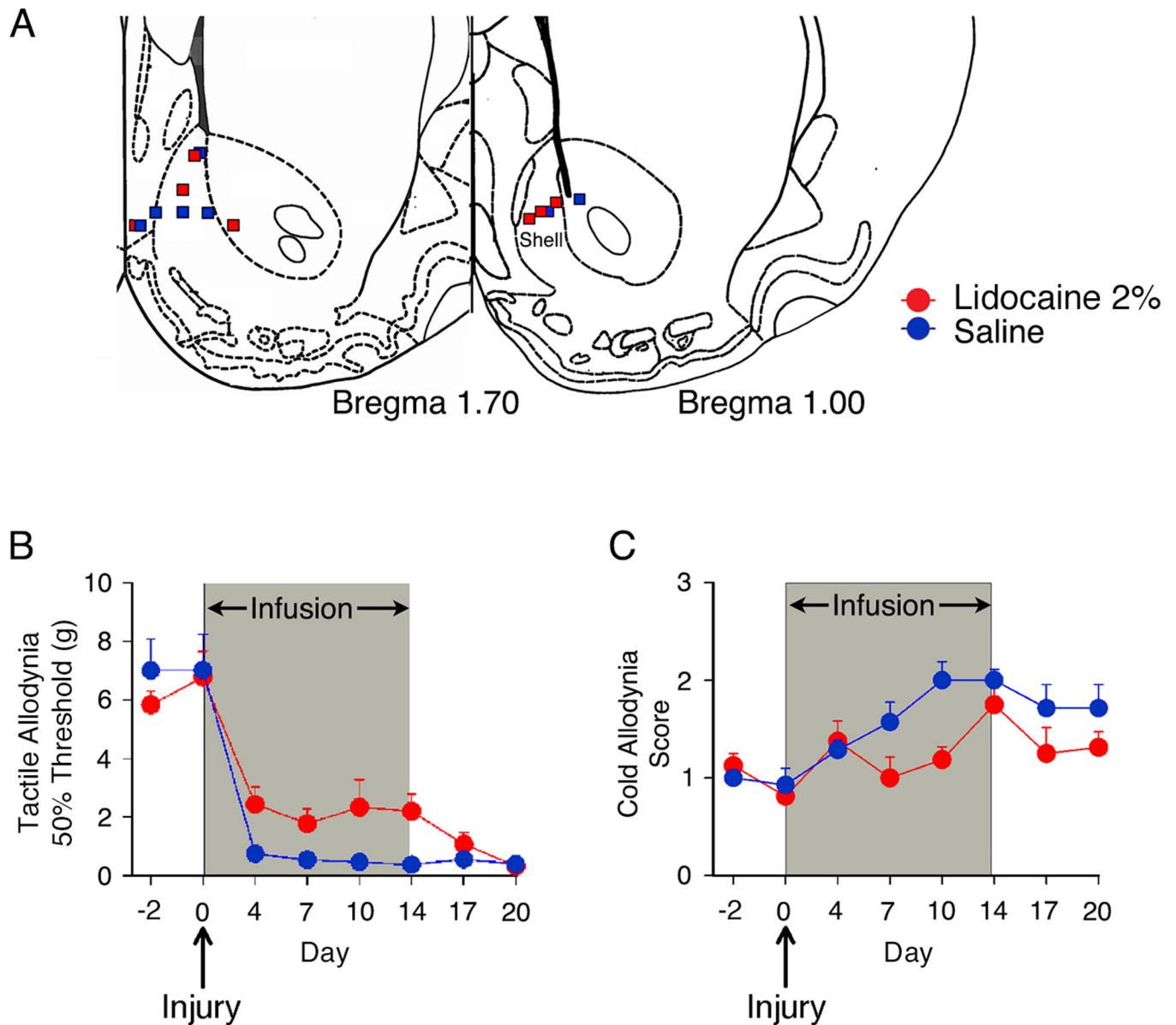
Fig. 8. Disruption of NAc neuronal activity reduces tactile and cold allodynia in SNI animals
(**A**) Locations of tips of mini pump cannula in NAc contralateral to peripheral nerve injury. Majority of tips are localized at medial shell of NAc. (**B**) Continuous infusion of Lidocaine for 14 days significantly reduced tactile allodynia, in comparison to the tactile allodynia of saline infused animals during treatment (P = 0.02). After cessation of treatment at Day14, the thresholds of the Lidocaine infused animals progressively returned to the levels of saline infused animals. (**C**) Chronic administration of Lidocaine also significantly reduced cold allodynia during the treatment period (P = 0.01).